GPS Solut
DOI 10.1007/s10291-011-0232-x

ORIGINAL ARTICLE

Apparent clock variations of the Block IIF-1 (SVN62) GPS satellite

Oliver Montenbruck · Urs Hugentobler · Rolf Dach · Peter Steigenberger · André Hauschild

Received: 11 April 2011 / Accepted: 8 June 2011

Abstract The Block IIF satellites feature a new generation of high-quality rubidium clocks for time and frequency keeping and are the first GPS satellites transmitting operational navigation signals on three distinct frequencies. We investigate apparent clock offset variations for the Block IIF-1 (SVN62) spacecraft that have been identified in L1/L2 clock solutions as well as the L1/L5-minus-L1/L2 clock difference. With peak-to-peak amplitudes of 10–40 cm, these variations are of relevance for future precision point positioning applications and ionospheric analyses. A proper characterization and understanding is required to fully benefit from the quality of the new signals and clocks. The analysis covers a period of 8 months following the routine payload activation and is based on GPS orbit and clock products generated by the CODE analysis center of the International GNSS Service (IGS) as well as triple-frequency observations collected with the CONGO network. Based on a harmonic analysis, empirical models are presented that describe the sub-daily variation of the clock offset and the inter-frequency clock difference. These contribute to a better clock predictability at timescales of several hours and enable a consistent use of L1/L2 clock products in L1/L5-based positioning.

O. Montenbruck (✉) · A. Hauschild
German Space Operations Center, Deutsches Zentrum für Luft- und Raumfahrt, 82230 Weßling, Germany
e-mail: oliver.montenbruck@dlr.de

U. Hugentobler · P. Steigenberger
Institut für Astronomische und Physikalische Geodäsie, Technische Universität München, Arcisstrasse 21, 80333 Munich, Germany

R. Dach
Astronomical Institute, University of Bern, Sidlerstrasse 5, 3012 Bern, Switzerland

Keywords GPS L5 · Block IIF · SVN62 · Rubidium clock · Allan variance · CONGO

Introduction

The latest generation of GPS satellites, termed Block IIF, provides a wide range of innovations and enhancements compared with the earlier Block IIA and Block IIR-A/B/M satellites (Dorsey et al. 2006; Braschak et al. 2010). From a civil user's point of view, the most important improvements are the addition of a new L5 signal as well as the use of an enhanced rubidium frequency standard.

The L5 signal is specifically designed for aeronautical safety-of-life applications. It is transmitted in the protected Aeronautical Radio Navigation Services (ARNS) frequency band and offers a higher robustness than the civil L2C signal due to its increased chipping rate and power level. Along with the existing L1 and L2 signals, the availability of a third frequency opens new prospects for fast ambiguity resolution in relative positioning (Teunissen et al. 2002), for integrity monitoring (Tsai et al. 2004), and for the analysis of ionospheric refraction effects (Spits and Warnant 2008). The new Block IIF rubidium frequency standard (RFS-IIF) is a successor of the Perkin-Elmer rubidium clocks that are presently in use onboard the Block IIR satellites. It offers a factor-of-two reduction of the white noise level over timescales of 100 s to 1 day, which is achieved through use of a xenon buffer gas and a thin-film filter for the Rb-D spectral lines in the improved physics package (Dupuis et al. 2010).

The first Block IIF satellite, known as IIF-1, SVN62, or PRN25, was launched on May 28, 2010, and set healthy for public use within 3 months. Despite the fact that the satellite flawlessly passed all in-orbit tests and perfectly

Published online: 16 July 2011

meets all spacecraft and navigation payload specifications, two surprising aspects were noted by the scientific community during the commissioning phase. First, an apparent inconsistency of the L_1, L_2, and L_5 carrier phase measurements at the 10-cm level was identified based on a geometry- and ionosphere-free linear combination of triple-frequency observations shortly after the permanent L5 activation on June 28, 2010 (Montenbruck et al. 2010a). This inconsistency can best be understood by a thermally dependent inter-frequency bias. It was particularly prominent at the time of its discovery, since SVN62 passed through the earth's shadow once every 12 h in the first weeks after launch.

Secondly, periodic variations of the L1/L2 clock solution of SVN62 with predominant 1/rev and 2/rev periodicities and amplitudes of about 0.5 ns (15 cm) were reported by Senior (2010) after activation of the rubidium clock in mid-July 2010. They result in a pronounced degradation of the Allan variance at time intervals of 1–12 h as compared to life tests of similar clocks carried out at the Naval Research Lab prior to the flight (Vannicola et al. 2010). While the SVN62 rubidium frequency standard clearly outperforms clocks of other GPS satellites at time intervals of less than an hour and beyond a day (Senior 2010; Dupuis et al. 2010), a clear "bump" in the Allan variance shows up at intermediate intervals, which limits the clock predictability at these timescales.

With the above background, we have monitored and analyzed the variation of the SVN62 clock offset along with the L1/L5-minus-L1/L2 clock difference over a period of 8 months after launch. The presentation starts with a discussion of linear measurement combinations from triple-frequency observations and their relation to clock offset and line bias determination. Subsequently, a harmonic analysis is performed and the seasonal dependence of the sub-daily variations is described by an empirical model in relation to the varying sun elevation above the orbital plane. Next, basic thermal considerations are presented to relate the observed clock and line bias variations to the sun–spacecraft–earth geometry and to explain the dominancy of 1/rev and 2/rev harmonics outside the eclipse season.

Multi-frequency measurement combinations

Following the standard GPS measurement model, the carrier phase measurements L_i ($i = 1, 2, 5$) collected on the L1, L2, and L5 frequencies may be described as

$$L_i = (\rho + cdt_{\mathrm{Rcv}} + T) + (-cdt + b_i) + (-I_1 \cdot f_1^2/f_i^2) + \mathrm{const} \tag{1}$$

where the additive constant reflects a signal- and pass-specific carrier phase ambiguity. The first bracket in (1) describes the contributions of the geometric range ρ, the receiver clock offset cdt_{Rcv}, and the tropospheric path delay T. The term cdt denotes the satellite clock offset term and has been grouped with a satellite-specific line bias b_i, which is considered to be both signal and time dependent. The third term, finally, describes the ionospheric phase advance, which is proportional to the L1 path delay I_1 and the inverse square of the signal frequency f_i.

When processing the ionosphere-free linear combination

$$\mathrm{IF}(L_i, L_j) = \frac{f_i^2}{f_i^2 - f_j^2} \cdot L_i - \frac{f_j^2}{f_i^2 - f_j^2} \cdot L_j \tag{2}$$

of dual-frequency phase observations as part of the GPS orbit and time determination, an estimate

$$\overline{cdt}_{ij} = cdt - \left(\frac{f_i^2}{f_i^2 - f_j^2} \cdot b_i - \frac{f_j^2}{f_i^2 - f_j^2} \cdot b_j \right) \tag{3}$$

of the clock offset is obtained, which differs from the true value by a linear combination of the individual phase biases.

Due to the presence of signal- or frequency-dependent biases $b_i(t)$, the processing of L1/L5 measurements may, in general, result in a different clock estimate than the processing of legacy L1/L2 observations. Combining (1)–(3), it can be recognized that the difference

$$\overline{cdt}_{15} - \overline{cdt}_{12} = \mathrm{IF}(L_1, L_2) - \mathrm{IF}(L_1, L_5) + \mathrm{const} \tag{4}$$

of the L1/L5 and L1/L2 clock offset estimates is equal to the difference of the ionosphere-free L1/L2 and L1/L5 carrier phase combinations up to a constant ambiguity term. The significance of this expression stems from the fact that the inter-frequency clock bias is directly observable from the triple-frequency carrier phase combination

$$\begin{aligned} \mathrm{DIF}(L_1, L_2, L_5) &= \mathrm{IF}(L_1, L_2) - \mathrm{IF}(L_1, L_5) \\ &= \left(\frac{f_1^2}{f_1^2 - f_2^2} - \frac{f_1^2}{f_1^2 - f_5^2} \right) \cdot L_1 \\ &\quad - \left(\frac{f_2^2}{f_1^2 - f_2^2} \right) \cdot L_2 + \left(\frac{f_5^2}{f_1^2 - f_5^2} \right) \cdot L_5 \end{aligned} \tag{5}$$

Similar to the triple-carrier combination introduced by Montenbruck et al. (2010a), (5) represents a geometry- and ionosphere-free linear combination of the L_1, L_2, and L_5 carrier phase combination. However, it employs a different normalization with roughly two times larger coefficients that is more suitable for clock-related analysis.

Considering both carrier phase and pseudorange measurements (P_i), the Melbourne–Wübbena combination

$$\mathrm{MW}(L_i, L_j, P_i, P_j) = \frac{f_i}{f_i - f_j} \cdot L_i - \frac{f_j}{f_i - f_j} \cdot L_j - \frac{f_i}{f_i + f_j} \cdot P_i - \frac{f_j}{f_i + f_j} \cdot P_j \tag{6}$$

Table 1 Linear combinations of triple-frequency GPS observations for clock and line bias analysis

Combination	Value
IF(L_1, L_2)	$+2.546\ L_1 - 1.546\ L_2$
IF(L_1, L_5)	$+2.261\ L_1 - 1.261\ L_5$
DIF(L_1, L_2, L_5)	$+0.285\ L_1 - 1.546\ L_2 + 1.261\ L_5$
MW(L_1, L_2, P_1, P_2)	$+4.529\ L_1 - 3.529\ L_2 - 0.562\ P_1 - 0.438\ P_2$
MW(L_1, L_5, P_1, P_5)	$+3.949\ L_1 - 2.949\ L_5 - 0.572\ P_1 - 0.428\ P_5$
MW(L_2, L_5, P_2, P_5)	$+24.00\ L_2 - 23.00\ L_5 - 0.511\ P_2 - 0.489\ P_5$

provides an independent way of forming geometry- and ionosphere-free linear observations. Numerical expressions for the individual combinations that can be formed from GPS L1, L2, and L5 measurements are summarized in Table 1. Due to the close proximity of the L2 and L5 frequencies, the MW combination for these signals amplifies carrier phase errors by more than a factor of 20 and thus enables an analysis of L_2 and L_5 line biases despite the presence of pseudorange noise and multipath errors. Unfortunately, the same does not hold for MW combinations involving the L1 frequency, and it is therefore not possible to unambiguously derive individual carrier phase line biases for each frequency from the available observations.

Data sets and processing

The present work makes use of "final" daily clock products with a 30-s sampling rate that have been generated by the Center for Orbit Determination in Europe (CODE) (Dach et al. 2009; Bock et al. 2009) based on dual-frequency (L1/L2) GPS observations of the International GNSS Service (IGS; Dow et al. 2009) network. Phase wind-up effects (Wu et al. 1993) are considered in the orbit and clock determination of CODE, assuming a nominal attitude of the GPS satellites (earth pointing $+z$-axis, sun perpendicular to y-axis in the $+x$ hemisphere). During the eclipse season, the actual SVN62 spacecraft orientation differs from this idealized model near noon and midnight turns due to limited physical rotation rates (Dilssner 2010). A partial degradation of the resulting clock solutions must therefore be expected in this period (Kouba 2009).

For the analysis of periodic clock variations, the relativistic J_2 contribution

$$c\delta t_{J_2}^{\mathrm{rel}} = -\frac{3}{2} J_2 \left(\frac{R_\oplus}{a}\right)^2 a\left(\frac{v}{c}\right) \sin^2 i \sin 2u \approx -0.02\ \mathrm{m} \cdot \sin 2u \tag{7}$$

(Kouba 2004) has been removed from the CODE clock solutions. The correction varies with the argument of latitude u and exhibits a 20 mm amplitude. It is not presently incorporated in the IGS processing standards and has no impact on computed positions if consistently ignored in both the GPS orbit/clock product generation and the precise point. However, it is of relevance for an improved estimate of the clock's intrinsic time and for a proper interpretation of 2/rev clock offset variations related to the varying sun aspect angle. The corrected clock solutions have, finally, been detrended by removing a drift and offset on a daily basis.

Triple-frequency observations of SVN62 have been obtained from the COperative Network for GIOVE observations (CONGO; Montenbruck et al. 2010b). The multi-GNSS network offered joint L1/L2/L5 GPS tracking from a total of 10 globally distributed stations at the time of the SVN62 launch and has since grown to a total of 16 contributing stations. This enabled a continuous coverage of the SVN62 satellite from at least a single station. Triple-frequency IF(L_1, L_2) − IF(L_1, L_5) combinations were first formed from the carrier phase measurements of each station on an epoch-by-epoch basis and grouped into passes based on a continuity test. Data were then combined into a single time series of the $c\overline{dt}_{15} - c\overline{dt}_{12}$ inter-frequency clock difference by adjusting pass-by-pass biases in a least-squares adjustment with zero-mean a priori constraint over a total arc of typically 3 days. In a similar way, continuous time series for the Melbourne–Wübbena combination (6) have been generated for specific periods. Differential phase wind-up effects (Wu et al. 1993) in the tri-carrier combination amount to 2 mm and have therefore been neglected, while the MW combination is rigorously free of such effects.

Exemplary results for the daily variation of the detrended L1/L2 clock offset and the L1/L5-minus-L1/L2 clock bias are provided in Figs. 1 and 2 for three selected 3-day periods in the second half of 2010. In all cases, periodic variations with dominating 1/rev and 2/rev contributions can clearly be recognized. The amplitude is lowest in mid-September, when the sun attained a maximum angle of 54° relative to the orbital plane of SVN62 and is only moderately larger in November at a sun angle of about 27°. The most pronounced variations are encountered in the eclipse phase (December 2010), where the dominating impact of the shadow transit is evident. Obviously, both the L1/L2 clock offset and the inter-frequency bias are subject to thermal variations with peak positive values related to a cooling of equipment and peak negative values reached after equipment warm-up. This is consistent with observations reported after first activation of the L5 payload, where a gradual decrease of the triple-carrier combination was encountered during the early days of operation (Montenbruck et al. 2010a).

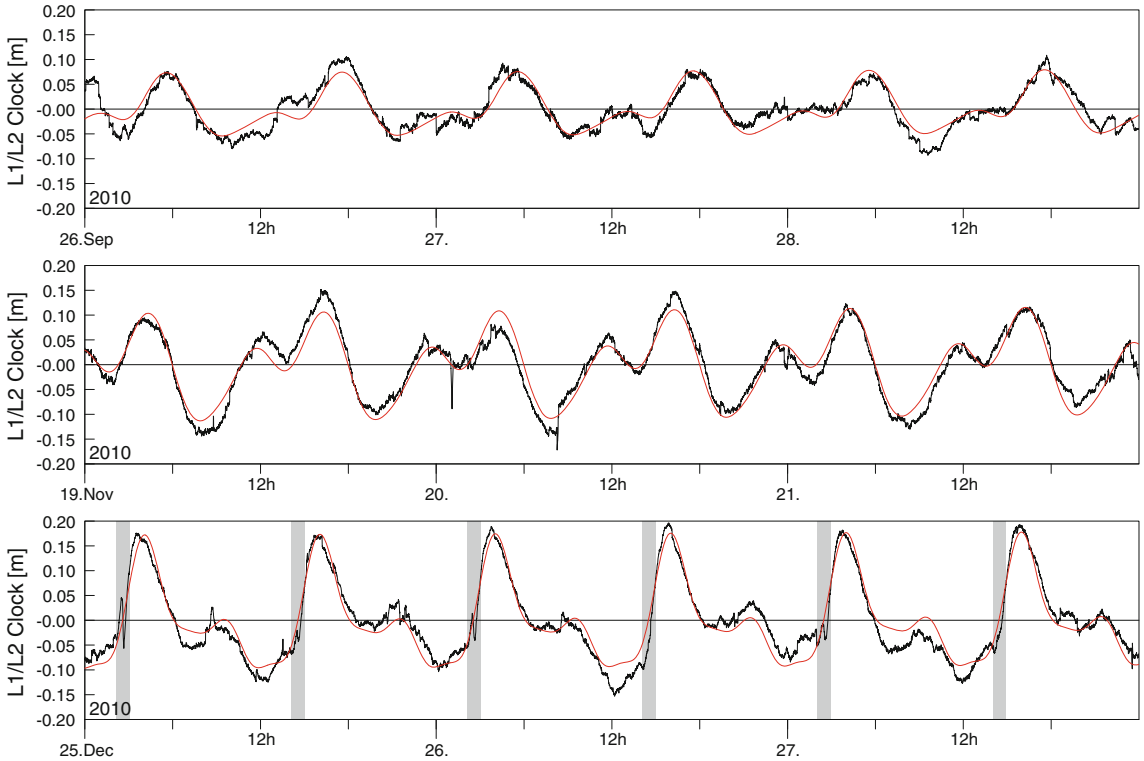

Fig. 1 Detrended SVN62 L1/L2 clock offset variation for selected 3-day arcs with high (*top*), medium (*center*), and low (*bottom*) sun angles relative to the orbital plane. *Gray bars* indicate eclipses, and *red lines* describe a harmonic fit including terms up to four times the orbital frequency

Harmonic analysis

In view of the clear orbital periodicity of the clock variations evidenced by Figs. 1 and 2, a harmonic analysis has been performed, in which the L1/L2 clock offset ($c\overline{dt}_{12}$) and the L1/L5 − L1/L2 inter-frequency difference ($c\overline{dt}_{15} - c\overline{dt}_{12}$) are each represented by a linear-plus-periodic model function of the form

$$f(t) = (a + b \cdot t) + \sum_{i=1}^{4} [c_i \cdot \cos(i\mu) + s_i \cdot \sin(i\mu)] \tag{8}$$

or, equivalently,

$$f(t) = (a + b \cdot t) + \sum_{i=1}^{4} A_i \cdot \sin(i\mu + \Phi_i) \tag{9}$$

The model incorporates harmonic terms up to four times the orbital frequency and is parameterized in terms of the orbit angle μ that is counted from the midnight line (i.e., the point of minimum sun–spacecraft–earth angle) and increases almost linearly with time (Fig. 3).

The harmonic coefficients c_i and s_i have been estimated from a least squares fit over consecutive 3-day data arcs over the first 8 months of SVN62 operations and are shown in Figs. 4 and 5 for the clock offset and the inter-frequency clock difference, respectively. While the clock coefficients exhibit a notably higher noise than those of the clock difference, the following common aspects may be noted:

- The coefficients depend primarily on the magnitude of the sun elevation above the orbital plane (β-angle, Fig. 3), even though a slight asymmetry with respect to a pure $|\beta|$ dependence can be suspected for the 1/rev harmonics.
- Outside the eclipse phase ($|\beta| > 14°$), the 3/rev and 4/rev terms can essentially be neglected. The amplitude of the first- and second-order harmonics ($i = 1, 2$) increases by a factor of 2–3 when proceeding from high to low sun elevations. Furthermore, the amplitude ratio s_i/c_i remains roughly constant in this region, indicating a constant phase Φ_i for these harmonics.
- During the eclipse phase ($|\beta| < 14°$), a steep peak in the clock offset and the inter-frequency clock difference can be noted that is triggered by the shadow entry but persists for a few hours after shadow exit (Figs. 1, 2). This reflects itself in a notable amplitude increase in proportion to the eclipse duration for all harmonics. Also, a change in the relative phases of the individual phases may be noted in comparison with the eclipse-free period.

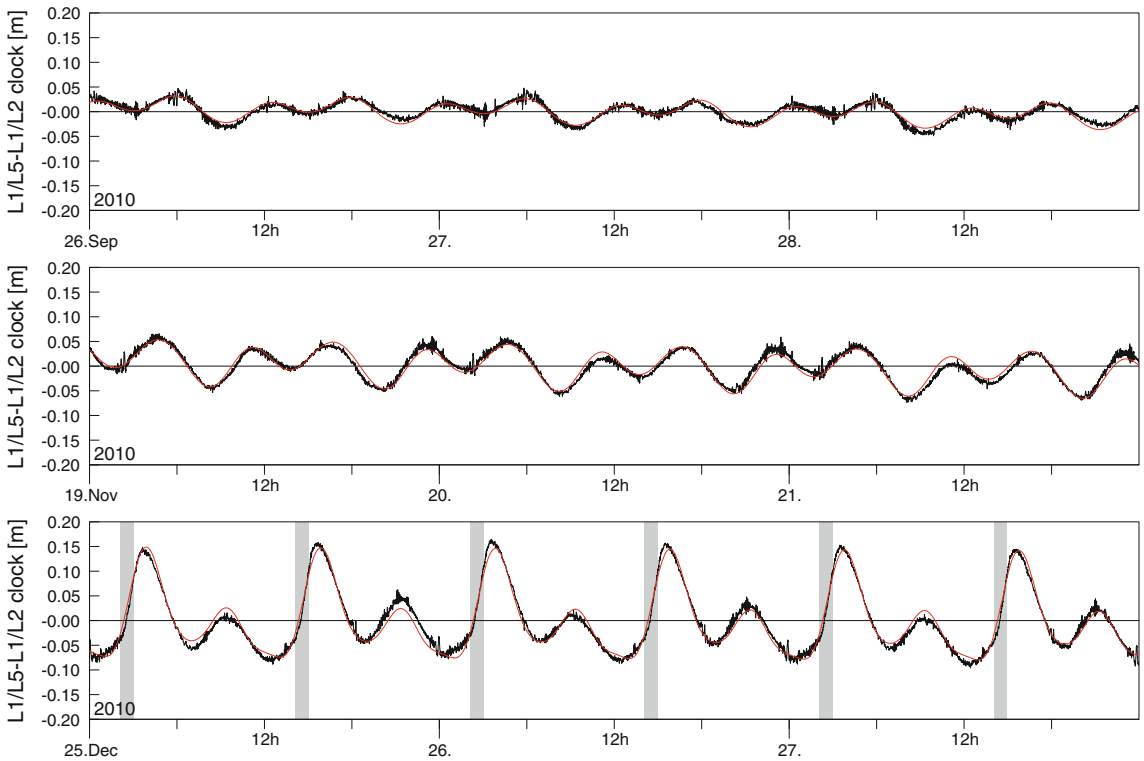

Fig. 2 Variation of the L1/L5-minus-L1/L2 clock offset difference of SVN62 as derived from triple-frequency carrier phase observations

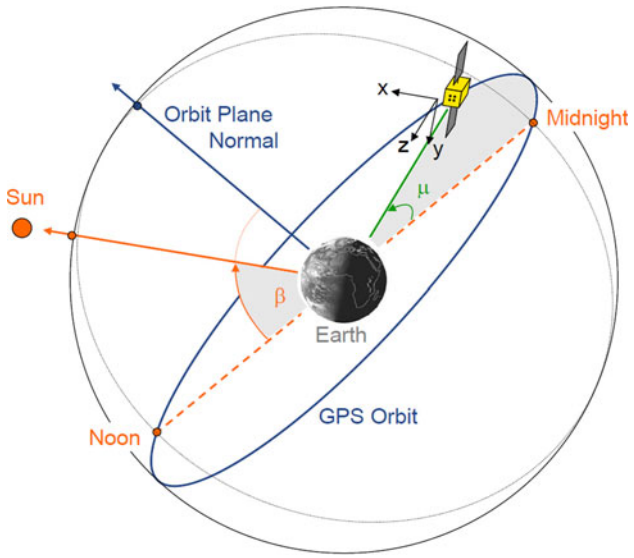

Fig. 3 GPS satellite orientation and angles describing the alignment of the sun, earth, satellite, and orbital plane

Based on the data in Figs. 4 and 5, approximate expressions for the harmonic coefficients in terms of $|\beta|$ have been established for the clock offset (Table 2) and the inter-frequency clock difference (Table 3). Favoring a very simple functional structure, linear approximations were used for the eclipse-free interval ($|\beta| > 14°$), while cubic or linear functions of $|\beta|$ were adjusted to represent the variation during the eclipse phase under the condition of continuity at the interval boundary. In case of the inter-frequency clock difference, an amplitude/phase representation was found to provide the most compact representation, whereas the Cartesian representation appeared preferable for the clock offset model.

On average, over the 8-month time interval, the L1/L5-minus-L1/L2 clock offset difference can be described by the above model with a typical accuracy of 1 cm rms. It thus provides a convenient way to translate legacy L1/L2 clock products for future users of L1/L5 receivers. These are expected to become a standard in aviation applications, and the need for creating distinct L1/L5 clock products for L1/L5 precise point positioning may become obsolete if the satellite-induced inter-frequency biases can be adequately described by a model.

As concerns the periodic variations of the L1/L2 clock solution, the corresponding model matches the actual variation over the test period with a representative accuracy of about 3 cm. This is clearly worse than obtained for the inter-frequency difference, but can be understood by the stochastic processes affecting the clock offset. Also, the clock offset determination process itself suffers from larger uncertainties than the determination of the L1/L5-minus-L1/L2 difference, which is directly observable from triple-frequency carrier phase measurements. This is particularly true for the eclipse phase, where a detailed attitude model

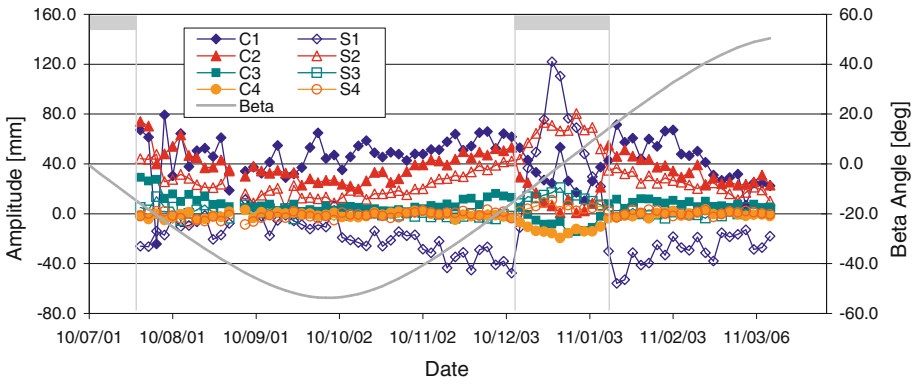

Fig. 4 Seasonal variation of harmonic coefficients for SVN62 L1/L2 clock offsets. *Shaded bars* indicate the eclipse periods

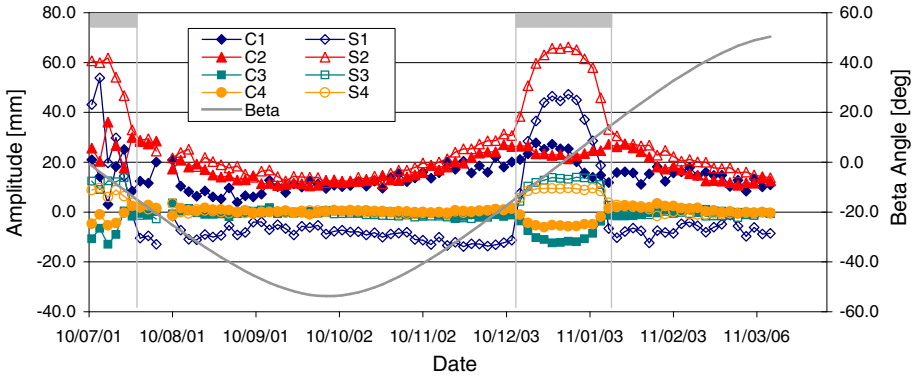

Fig. 5 Seasonal variation of harmonic coefficients for SVN62 L1/L5−L1/L2 inter-frequency clock offset difference. *Shaded bars* indicate the eclipse periods

Table 2 Harmonic coefficients of periodic L1/L2 clock offset variation

Harmonics	Cosine coefficient (mm)	Sine coefficient (mm)
1/rev	$c_1 = \begin{cases} 20 + 40 \cdot B_1^3 \\ 60 - 20 \cdot B_2 \end{cases}$	$s_1 = \begin{cases} 125 - 160 \cdot B_1 \\ -35 + 25 \cdot B_2 \end{cases}$ for $\begin{cases} \lvert\beta\rvert \le 14^\circ \\ \lvert\beta\rvert > 14^\circ \end{cases}$
2/rev	$c_2 = \begin{cases} 5 + 50 \cdot B_1^3 \\ 55 - 30 \cdot B_2 \end{cases}$	$s_2 = \begin{cases} 72 - 32 \cdot B_1^3 \\ 40 - 30 \cdot B_2 \end{cases}$ for $\begin{cases} \lvert\beta\rvert \le 14^\circ \\ \lvert\beta\rvert > 14^\circ \end{cases}$
3/rev	$c_3 = \begin{cases} -12 + 27 \cdot B_1^3 \\ 15 - 10 \cdot B_2 \end{cases}$	$s_3 = \begin{cases} 17 - 15 \cdot B_1^3 \\ 2 - 4 \cdot B_2 \end{cases}$ for $\begin{cases} \lvert\beta\rvert \le 14^\circ \\ \lvert\beta\rvert > 14^\circ \end{cases}$
4/rev	$c_4 = \begin{cases} -17 + 15 \cdot B_1^3 \\ -2 \end{cases}$	$s_4 = \begin{cases} 7 - 9 \cdot B_1^3 \\ -2 \end{cases}$ for $\begin{cases} \lvert\beta\rvert \le 14^\circ \\ \lvert\beta\rvert > 14^\circ \end{cases}$
With	$B_1 = \lvert\beta\rvert/14^\circ\,,\ \ B_2 = (\lvert\beta\rvert - 14^\circ)/40^\circ$	

Table 3 Harmonic coefficients of the L1/L5-minus-L1/L2 clock offset difference

Harmonics	Amplitude (mm)	Phase
1/rev	$A_1 = \begin{cases} 50 - 30 \cdot B_1^3 \\ 20 - 8 \cdot B_2 \end{cases}$	$\Phi_1 = \begin{cases} +30^\circ \\ +120^\circ \end{cases}$ for $\begin{cases} \lvert\beta\rvert \le 14^\circ \\ \lvert\beta\rvert > 14^\circ \end{cases}$
2/rev	$A_2 = \begin{cases} 68 - 26 \cdot B_1^3 \\ 42 - 27 \cdot B_2 \end{cases}$	$\Phi_2 = \begin{cases} +20^\circ \\ +40^\circ \end{cases}$ for $\begin{cases} \lvert\beta\rvert \le 14^\circ \\ \lvert\beta\rvert > 14^\circ \end{cases}$
3/rev	$A_3 = \begin{cases} 20 - 18 \cdot B_1^3 \\ 2 - 2 \cdot B_2 \end{cases}$	$\Phi_3 = \begin{cases} -30^\circ \\ 0^\circ \end{cases}$ for $\begin{cases} \lvert\beta\rvert \le 14^\circ \\ \lvert\beta\rvert > 14^\circ \end{cases}$
4/rev	$A_4 = \begin{cases} 11 - 9 \cdot B_1^3 \\ 2 - 2 \cdot B_2 \end{cases}$	$\Phi_4 = \begin{cases} -40^\circ \\ 0^\circ \end{cases}$ for $\begin{cases} \lvert\beta\rvert \le 14^\circ \\ \lvert\beta\rvert > 14^\circ \end{cases}$
With	$B_1 = \lvert\beta\rvert/14^\circ\,,\ \ B_2 = (\lvert\beta\rvert - 14^\circ)/40^\circ$	

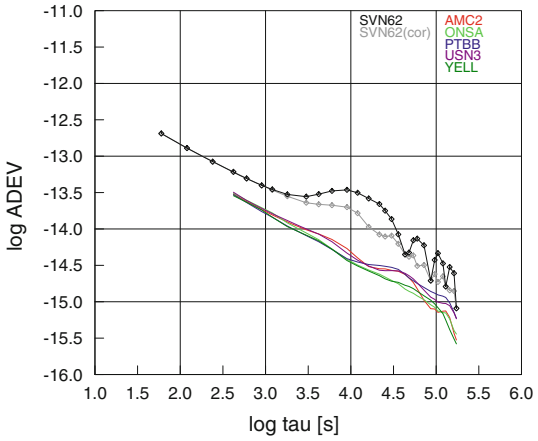

Fig. 6 Allan deviation of SVN62 rubidium clock in GPS week 1620 based on CODE final products (*black dotted line*) and after correction with empirical clock offset model (*gray dotted line*). For reference, the solid colored lines provide the Allan deviation of selected IGS reference stations connected to high-precision masers

would be required in the orbit and clock determination to properly describe the associated phase wind-up effects.

To assess the benefit of a model-based prediction of the periodic clock variations, the overlapping Allan deviation (ADEV; Riley 2008) of the CODE clock products for SVN62 has been computed for a 1-week test arc (GPS week 1620, January 23–29, 2011). In this time period, the β-angle varied between 24° and 29° and the periodic clock variations exhibited a peak-to-peak amplitude of about 20 cm. Daily offsets were adjusted to the CODE clock solutions to remove day-boundary discontinuities, and the SVN62 clock solution was referred to a single highly stable ground clock (Herstmonceux) over the entire arc. Furthermore, the resulting solution was detrended through a fifth-order polynomial adjusted over the entire week. We also recall that the relativistic J_2 correction (7) has been applied to the CODE clock data which would otherwise exhibit a superimposed 2/rev variation with 20 mm amplitude.

As illustrated in Fig. 6, the ADEV of the SVN62 clock in the considered period follows an approximate power law

$$\mathrm{ADEV}(\tau) \approx 1.4 \times 10^{-13} \cdot (\tau/100\ \mathrm{s})^{-0.6} \tag{10}$$

for time intervals τ of 30 s to 2000 s and is merely 2 times larger than that of high performance ground clocks. For longer timescales, the ADEV increases again and exhibits a local maximum near $\tau = 10{,}000$ s. Thereafter, steep minima are attained at the orbital period (approx. 43,080 s) and integer multiples thereof, which clearly reflects the presence of 1/rev clock variations. When correcting the clock data with the empirical harmonic model, the "bump" between 3,000 and 40,000 s is notably flattened and the ADEV improves by a factor of two or more. A similar improvement can also be recognized for timescales of 0.5–2 days.

Aside from the triple-frequency carrier phase combination and the L1/L2 clock offset, periodic variations are also evident for the L2/L5 Melbourne–Wübbena combination (6). Line biases in the L_2 and L_5 carrier phase measurements are strongly amplified in this combination (Table 1) and amplitudes of 1/rev and 2/rev terms at the meter level are encountered in this case. Altogether, the triple-carrier phase combination, the L2/L5 Melbourne–Wübbena combination and the L1/L2 clock variation provide three independent observations for the line biases b_1, b_2, and b_5 as well as the clock offset cdt. As an example, the linear equations

$$\begin{pmatrix} +0.285 & -1.546 & +1.261 & 0 \\ 0 & 24 & -23 & 0 \\ -2.546 & +1.546 & 0 & -1 \end{pmatrix} \cdot \begin{pmatrix} b_1 \\ b_2 \\ b_5 \\ cdt \end{pmatrix} = \begin{pmatrix} +26.9 & +34.1 & +23.8 & +57.8 \\ -501 & -613 & -416 & -1035 \\ +52.1 & +45.8 & +15.4 & +58.4 \end{pmatrix}_{[\mathrm{mm}]} \cdot \begin{pmatrix} \cos\mu \\ \sin\mu \\ \cos 2\mu \\ \sin 2\mu \end{pmatrix} + \begin{pmatrix} \varepsilon_{\mathrm{DIF3}} \\ \varepsilon_{\mathrm{MW}(L2,L5)} \\ \varepsilon_{cdt(L1,L2)} \end{pmatrix} \tag{11}$$

are obtained from the harmonic analysis of the respective measurements for a 3-day interval during the eclipse phase in mid-December 2010 ($\beta = -10.3° \ldots -7.8°$). Approximate noise levels of

$$\begin{pmatrix} \varepsilon_{\mathrm{DIF3}} \\ \varepsilon_{\mathrm{MW}(L2,L5)} \\ \varepsilon_{cdt(L1,L2)} \end{pmatrix} \approx \begin{pmatrix} 5 \\ 100 \\ 10 \end{pmatrix}_{[\mathrm{mm}]} \tag{12}$$

can be inferred from the scatter of the individual harmonic coefficients as determined from different data batches and the overall goodness of fit of the harmonic representation of the measurement combination.

Evidently, three equations are insufficient to solve for four unknown parameters and further information would be required to discriminate between line bias variations and physical clock variations. It can be verified, though, that the above observations are compatible with a vanishing clock variation ($cdt = 0$), in which case line bias variations with amplitudes of 20–70 mm and a formal uncertainty of 20 mm are obtained for the respective 1/rev and 2/rev harmonics on the L1, L2, and L5 carriers. On the other hand, the observations are likewise compatible with the assumption of vanishing line biases in both the L1 and L2

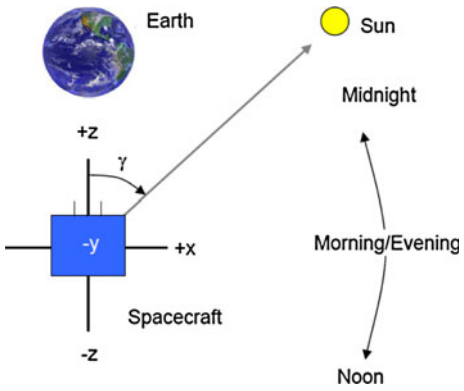

Fig. 7 Sun illumination of the GPS spacecraft

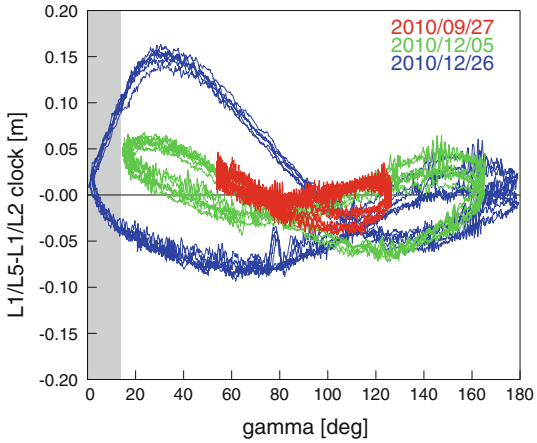

Fig. 8 Variation of the L1/L5-minus-L1/L2 clock difference with the sun–spacecraft–earth angle (γ) for selected 3-day arcs at maximum β-angle ($\beta = -54°$; *red*), at the start of the eclipse season ($\beta = -14°$; *green*), and at the center of the eclipse phase ($\beta = 0°$; *blue*). At low γ angles, the curve is traversed in a clockwise manner

carriers ($b_1 = b_2 = 0$). The observed variations in the triple-frequency combination would then reflect the changing L5 carrier phase bias, while the apparent L1/L2 clock offset $c\overline{dt}_{12}$ would be identical to the actual clock offset cdt.

Thermal considerations

The dominant β-angle dependency and the impact of eclipses strongly suggest satellite internal temperature variations due to varying sun illumination as the root cause of the observed clock offset and inter-frequency clock bias variations. The GPS-specific attitude control concept implies that the sun direction is always contained in the x/z-plane of the spacecraft. In the course of each orbit, the sun direction vector oscillates about the $+x$-axis (Fig. 7) and the sun–spacecraft–earth angle γ varies between a minimum of $|\beta|$ at midnight ($\mu = 0°$) and a maximum of $180° - |\beta|$ at noon ($\mu = 180°$). Accordingly, the $+x$ panel remains continuously sun-lit (except during eclipses), whereas the $+z$ and $-z$ panels are only illuminated during one half of each orbit centered on midnight and noon, respectively. The $+y$ and $-y$ panels always see the sun at a zero elevation angle except during deviations from the nominal attitude that may occur during noon and midnight turns at low β-angles due to limited yaw slew rates (Dilssner 2010).

While the illumination itself depends exclusively on the sun–spacecraft–earth angle, the same does not hold for the observed clock offset and inter-frequency bias. As illustrated in Fig. 8 for the variation of $c\overline{dt}_{15} - c\overline{dt}_{12}$ versus γ, a distinct figure-of-eight shape is obtained, which evidences a delayed response of the observed clock offset difference to the sun illumination. This hysteresis is likewise indicated by the relative phase shift of the 1/rev and 2/rev harmonics (Table 3).

To better understand the observed variations, we consider a basic model of the spacecraft heating by the sun. The rate of energy absorbed by each panel depends exclusively on γ and is proportional to the projection of the sun direction unit vector on the respected surface:

$$\dot{Q}_{+z,\mathrm{in}} \propto \max(\cos(\gamma), 0) \quad \dot{Q}_{-z,\mathrm{in}} \propto \max(-\cos(\gamma), 0)$$
$$\dot{Q}_{+x,\mathrm{in}} \propto \sin(\gamma) \tag{13}$$

On average, the incoming energy is compensated by dissipation and re-radiation and a constant rate $\dot{Q}_{\mathrm{out}} = \overline{\dot{Q}_{\mathrm{in}}}$ can be assumed in the simplest case. The panel temperature is proportional to the stored energy Q and is thus obtained from the time integral of the irradiance:

$$\Delta T \propto Q = \int (\dot{Q}_{\mathrm{in}} - \overline{\dot{Q}_{\mathrm{in}}})dt \tag{14}$$

Figure 9 illustrates the modeled irradiance ($\dot{Q}_{\mathrm{in}} - \overline{\dot{Q}_{\mathrm{in}}}$) and the associated temperature variation for each of the three panels over a full orbit in case of high and low β-angles. It can be recognized that the $+x$ panel temperature variation exhibits a pronounced 2/rev periodicity, whereas the $+z$ and $-z$ panels show a dominant 1/rev temperature variation (in anti-phase). In addition, a smaller (20%) variation at twice the orbital frequency is obtained with an identical phase for both panels. On the other hand, no relevant 3/rev or 4/rev contributions are observed, which is consistent with the lack of such terms in the variations of the clock offset ($c\overline{dt}_{12}$) and the inter-frequency difference ($c\overline{dt}_{15} - c\overline{dt}_{12}$) outside the eclipse period. Furthermore, the simple thermal model offers a qualitative explanation for the changing amplitude of the 1/rev and 2/rev variations (Tables 2, 3), which increase by a factor of 2–3 when changing from high sun elevations ($\beta = 54°$) to low elevations ($\beta = 14°$) in the eclipse-free season.

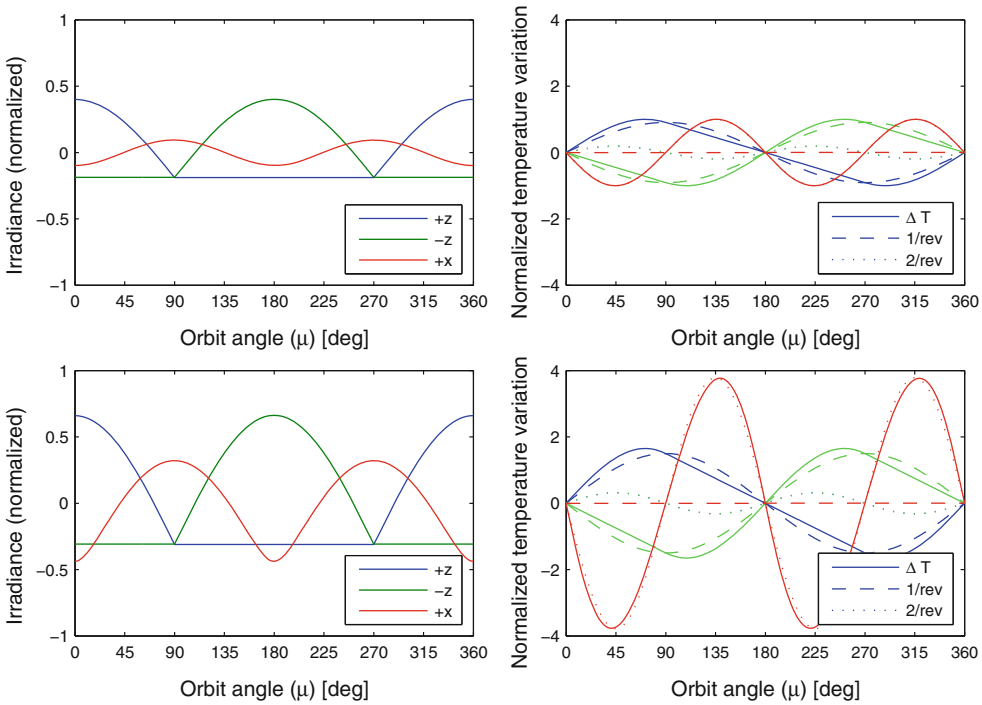

Fig. 9 Modeled irradiance (*left*) and temperature variations ΔT of the $+z$ (*blue*), $+x$ (*red*) and $-z$ (*green*) panels for different sun elevations above the orbital plane (*top*: $\beta = 54°$; *bottom*: $\beta = 14°$). *Dotted and dashed lines* illustrate the decomposition into 1/rev and 2/rev harmonics

Unfortunately, it is difficult to gain further insight from the model without a more detailed knowledge of the internal structure and thermal characteristics of the GPS satellite. Fundamentally, periodic surface temperature changes will propagate into the spacecraft body with an attenuation and delay, i.e. phase shift, that both depend on the frequency of these variations and the material properties (Alonso and Finn, 1967). On the Block IIF satellites, the atomic clocks as well as the L1 transmitter are mounted on the $-y$ side of the spacecraft and the opposite ($+y$) panel holds the L2 and L5 transmitters (Dorsey et al. 2006). From the above considerations, we can expect a superposition of 1/rev and 2/rev harmonics in the temperature of each of these navigation payload elements. Amplitudes and phases of these harmonics will be different for the individual devices but cannot be predicted without further information.

Discussion

As shown by Senior et al. (2008) based on a long-term spectral analysis of precise GPS ephemeris products, orbital harmonics with amplitudes of up to several nanoseconds can be identified in the observed clock offsets of all generations of GPS satellites. The amplitude of these sub-daily harmonics exhibits evident seasonal variations and increases during the eclipse phase. Despite notable improvements in the Block IIF rubidium clock with respect to its predecessors, clock variations with orbital and sub-orbital periodicity are likewise observed for this latest type of GPS satellites. However, the harmonic perturbations exceed the stochastic clock variations for the first Block IIF spacecraft in view of the high clock quality and become well observable even in shorter data arcs. For the first time, a study of inter-frequency biases independent of the physical clock behavior is, furthermore, enabled through the availability of triple-frequency measurements.

Fundamentally, orbital harmonics in the observed GPS clock offset solution may be caused through coupling with orbit determination uncertainties, oscillator frequency variations and line bias variations. GPS orbit determination errors are less than a few centimeters for current precise orbit products (Griffiths and Ray 2009) and typically dominated by 1/rev periods. A possible contamination of the clock solution with once-per-rev orbit errors must therefore be assumed (Senior et al. 2008), but 2/rev harmonics are considered to be mostly unaffected. As regards a thermal sensitivity of the atomic frequency standard, timing errors of ± 0.25 ns (± 7.5 cm) have been predicted by Wu (1996) for the Block IIR satellites based on an expected temperature variation of ± 2.5 K outside eclipses. Following Dupuis et al. (2010), the rubidium clocks of the Block IIF satellites are mounted on a thermally isolated sub-panel (along with the frequency distribution unit) for which a peak-to-peak temperature variation of less than 0.5 K has been observed in SVN62 onboard measurements. In addition, the new clock benefits from a baseplate temperature controller (BTC), which further reduces the sensitivity to external temperature variations by up to a factor of 50. These numbers would suggest a negligible

contribution of temperature-induced frequency variations on the observed variance of the apparent SVN62 clock, but more detailed information and measurements appear necessary to substantiate this view.

Regarding the impact of temperature-dependent line biases, it is important to note that the inter-frequency clock difference is derived from geometry-free observations and therefore fully independent of orbit errors or physical clock offset variations. The triple-frequency carrier phase combination therefore provides an unambiguous evidence for the presence of thermally induced line bias variations in at least some of the three carriers. Similar considerations hold for the dual-frequency L2/L5 Melbourne–Wübbena combination. Despite the availability of triple-frequency observations and multiple linear combinations, it is not possible, though, to uniquely separate the line biases and physical clock offset variations. The observation types considered in the present study (i.e., the L1/L2 clock solutions, the triple-carrier combination, and the L2/L5 MW combination) are generally compatible with the assumption of a vanishing oscillator frequency variation, and the observed periodic variations might thus be caused exclusively by line bias variations. However, the validity of this assumption cannot be assessed due to a lack of public information on the Block IIF navigation payload characteristics and the satellite internal temperature variations. Such measurements are strongly encouraged to identify and potentially remove the root cause of the Block IIF apparent clock variations.

Summary and conclusions

An analysis of apparent clock variations of the first Block IIF satellite SVN62 has been performed. Orbit-periodic variations have been characterized for the apparent L1/L2 clock offset of the new rubidium frequency standard and the L1/L5-minus-L1/L2 clock difference. A thermal origin of these variations is evidenced by eclipse transits and the observed dependence of the individual harmonics on the sun elevation above the orbital plane.

The inter-frequency clock difference of 10–20 cm is decoupled from the actual oscillator performance and can exclusively be attributed to line bias variations in the radio frequency chain. An empirical model is established to describe the orbital and seasonal variations with a representative accuracy of 30 ps (1 cm). This will enable a consistent use of legacy L1/L2 clock products for future aviation users with L1/L5-only receivers. In addition, knowledge of the inter-frequency biases is of relevance for ionospheric investigations using triple-frequency measurements.

Concerning the observed variations of the L1/L2 clock solution, both thermally induced oscillator frequency variations as well as frequency-dependent line bias variations in the radio frequency chain can be suspected. However, the available measurements do not allow a conclusive discrimination of the two contributions. Using a harmonic analysis, the periodic variations of the apparent clock can be modeled with an accuracy of about 0.1 ns (3 cm). Even though the root cause of the apparent clock variation remains unclear, a clock correction based on the empirical model is shown to notably reduce the Allan variance at timescales of 1–12 h. It may thus contribute to improved clock predictions over sub-daily intervals and to extending the validity of broadcast clocks.

Acknowledgments The authors acknowledge the vital role of the International GNSS Service to this analysis. Orbit and clock solutions for SVN62 have been contributed by the Center for Orbit Determination in Europe (CODE) based on observations of the IGS network. CODE is a joint venture between the Astronomical Institute of the University of Bern (AIUB, Bern, Switzerland), the Federal Office of Topography (swisstopo, Wabern, Switzerland), the Federal Agency for Cartography and Geodesy (BKG, Frankfurt, Germany), and the Institut für Astronomische und Physikalische Geodäsie of the Technische Universität München (IAPG/TUM, Munich, Germany). It acts as a global analysis center of the IGS since June 1992. Triple-frequency observations have been provided by the CONGO multi-GNSS network. The contributions of all network partners (Deutsches Zentrum für Luft- und Raumfahrt, Bundesamt für Kartographie und Geodäsie, Technische Universität München, Deutsches GeoForschungsZentrum, Centre National d'Etudes Spatiales, Geoscience Australia) and local station hosts are gratefully acknowledged.

References

Alonso M, Finn EJ (1967) Fundamental university physics, vol II, fields and waves. Addison-Wesley, Reading

Bock H, Dach R, Jäggi A, Beutler B (2009) High-rate GPS clock corrections from CODE: support of 1 Hz applications. J Geodesy 83(11):1083–1094. doi:10.1007/s00190-009-0326-1

Braschak M, Brown H Jr., Carberry J, Grant T, Hatten G, Patocka R, Watts E (2010) GPS IIF satellite overview, ION-GNSS-2010, 21–24 Sept 2010, Portland, OR

Dach R, Brockmann E, Schaer S, Beutler G, Meindl M, Prange L, Bock H, Jäggi A, Ostini L (2009) GNSS processing at CODE: status report. J Geodesy 83(3–4):353–365. doi:10.1007/s00190-008-0281-2

Dilssner F (2010) GPS IIF-1 satellite—antenna phase center and attitude modeling. InsideGNSS, Sept 2010, pp 59–64

Dorsey AJ, Marquis WA, Fyfe PM, Kaplan ED, Wiederholt LF (2006) GPS system segments. In: Kaplan ED, Hegarty CJ (eds) Understanding GPS—principles and applications, 2nd edn. Artech House, Norwood, pp 67–112

Dow JM, Neilan RE, Rizos C (2009) The international GNSS service in a changing landscape of global navigation satellite systems. J Geodesy 83(3–4):191–198. doi:10.1007/s00190-008-0300-3

Dupuis RT, Lynch TJ, Vaccaro JR, Watts ET (2010) Rubidium frequency standard for the GPS IIF program and modifications for the RAFSMOD program. ION-GNSS-2010, 21–24 Sept 2010, Portland, OR

Griffiths J, Ray JR (2009) On the precision and accuracy of IGS orbits. J Geodesy 83(3–4):277–287. doi:10.1007/s00190-008-0237-6

Kouba J (2004) Improved relativistic clock correction due to earth oblateness. GPS Solut 8(3):170–180. doi:10.1007/s10291-004-0102-x

Kouba J (2009) A simplified yaw-attitude model for eclipsing GPS satellites. GPS Solut 13:1–12. doi:10.1007/s10291-008-0092-1

Montenbruck O, Hauschild A, Steigenberger P, Langley RB (2010a) Three's the challenge: a close look at GPS SVN62 triple-frequency signal combinations finds carrier-phase variations on the new L5. GPS World 21(8):8–19

Montenbruck O, Hauschild A, Hessels U (2010b) Characterization of GPS/GIOVE sensor stations in the CONGO network. GPS Solut 15(3):193–205. doi:10.1007/s10291-010-0182-8

Riley WR (2008) Handbook of frequency stability analysis, NIST special publication 1065. National Institute of Standards and Technology, Boulder, CO

Senior K (2010) SVN62 clock analysis using IGS data, IGSMAIL-6218, 6 Aug 2010, http://igscb.jpl.nasa.gov/pipermail/igsmail/2010/000051.html

Senior K, Ray JR, Beard RL (2008) Characterization of periodic variations in the GPS satellite clocks. GPS Solut 12(3):211–225. doi:10.1007/s10291-008-0089-9

Spits J, Warnant R (2008) Total electron content monitoring using triple frequency GNSS data: a three-step approach. J Atmospheric Solar-Terr Phys 70(15):1885–1893. doi:10.1016/j.jastp.2008.03.007

Teunissen PJG, Joosten P, Tiberius C (2002) A comparison of TCAR, CIR and LAMBDA GNSS ambiguity resolution. ION-GPS-2002, Portland, OR, pp 2799–2808

Tsai Y-H, Chang F-R, Yang W-C, Ma C-L (2004) Using multi-frequency for GPS positioning and receiver autonomous integrity monitoring. In: Proceedings of the 2004 IEEE international conference on control applications, Taipei, Taiwan, 2–4 Sept 2004

Vannicola F, Beard R, White J, Senior K, Kubik A, Wilson D (2010) GPS Block IIF rubidium frequency standard life test. ION-GNSS-2010, 21–24 Sept 2010, Portland, OR

Wu A (1996) Performance evaluation of the GPS Block IIR time keeping system. In: Breakiron L (ed) Proceedings of the 28th annual precise time and time interval applications and planning meeting. US Naval Observatory, Reston, pp 441–453

Wu JT, Wu SC, Hajj GA, Bertiger WI, Lichten SM (1993) Effects of antenna orientation on GPS carrier phase. Manuscripta Geodaetica 18:91–98

Author Biographies

Dr. Oliver Montenbruck is head of the GNSS Technology and Navigation Group at DLR's German Space Operations Center, where he started work as a flight dynamics analyst in 1987. His current research activities comprise space-borne GNSS receiver technology, autonomous navigation systems, spacecraft formation flying, precise orbit determination, and multiconstellation GNSS.

Dr. Urs Hugentobler is a full professor since 2006 at the Institute for Astronomical and Physical Geodesy of Technische Universität München, Germany, and head of the Research Establishment Satellite Geodesy. His research activities focus on precise applications of GNSS such as positioning, precise orbit determination, reference frame realization, and time transfer.

Rolf Dach received his Ph.D. thesis in geodesy at the Institut für Planetare Geodäsie of the University of Technology in Dresden, Germany. Since 1999, he has been working as a scientist at AIUB, where he is the head of the GNSS Research Group since 2006. He leads the development of the Bernese Software package and is responsible for the activities of the CODE analysis center of the IGS.

Dr. Peter Steigenberger works at the Institute of Astronomical and Physical Geodesy of Technische Universität München (TUM, Munich, Germany). His current research interests include global GNSS solutions and the analysis of the GNSS-derived parameter time series, e.g., troposphere zenith delays, station coordinates, satellite orbits, and Earth rotation parameters.

Dr. André Hauschild is a scientific staff member at DLR's German Space Operations Center (GSOC). His field of work focuses on precise real-time orbit and clock estimation for GNSS satellites as well as multi-GNSS processing using modernized GPS and new satellite navigation systems.